Published in final edited form as:
Neuroimage. 2012 April 2; 60(2): 1006–1014. doi:10.1016/j.neuroimage.2012.01.053.

T_2* mapping and B_0 orientation-dependence at 7 T reveal cyto- and myeloarchitecture organization of the human cortex

J. Cohen Adad[a,b,*], **J.R. Polimeni**[a,b], **K.G. Helmer**[a,b], **T. Benner**[a,b], **J.A. McNab**[a,b], **L.L. Wald**[a,b,c], **B.R. Rosen**[a,b], and **C. Mainero**[a,b]

[a] A.A. Martinos Center for Biomedical Imaging, Dept. of Radiology, Massachusetts General Hospital, Charlestown, MA, USA

[b] Harvard Medical School, Boston, MA, USA

[c] Harvard-MIT Division of Health Sciences and Technology, MIT, Cambridge, MA, USA

Abstract

Ultra-high field MRI (≥7 T) has recently shown great sensitivity to depict patterns of tissue microarchitecture. Moreover, recent studies have demonstrated a dependency between T_2* and orientation of white matter fibers with respect to the main magnetic field B_0. In this study we probed the potential of T_2* mapping at 7 T to provide new markers of cortical architecture. We acquired multi-echo measurements at 7 T and mapped T_2* over the entire cortex of eight healthy individuals using surface-based analysis. B_0 dependence was tested by computing the angle θ_z between the normal of the surface and the direction of B_0, then fitting T_2*(θ_z) using model from the literature. Average T_2* in the cortex was 32.20+/−1.35 ms. Patterns of lower T_2* were detected in the sensorimotor, visual and auditory cortices, likely reflecting higher myelin content. Significantly lower T_2* was detected in the left hemisphere of the auditory region (p<0.005), suggesting higher myelin content, in accordance with previous investigations. B_0 orientation dependence was detected in some areas of the cortex, the strongest being in the primary motor cortex (ΔR_2*=4.10 Hz). This study demonstrates that quantitative T_2* measures at 7 T MRI can reveal patterns of cytoarchitectural organization of the human cortex *in vivo* and that B_0 orientation dependence can probe the coherency and orientation of gray matter fibers in the cortex, shedding light into the potential use of this type of contrast to characterize cyto-/myeloarchitecture and to understand the pathophysiology of diseases associated with changes in iron and/or myelin concentration.

Keywords

Ultra-high field MRI; Cytoarchitecture; Myeloarchitecture T_2*; Susceptibility

Introduction

The characterization of the cyto- and myeloarchitecture of the cerebral cortex *in vivo* has been an inexhaustible field of research over the past century, as it can provide new insights into structure–function relationships in the brain and help guide the development of cortical atlases for the study of functional specialization (Eickhoff et al., 2005; Geyer et al., 2011; Glasser and Van Essen, 2011; Van Essen, 2005; Zilles, 2004). Cytoarchitectonics refers to

*Corresponding author at: A.A. Martinos Center for Biomedical Imaging, Massachusetts General Hospital, Building 149, Thirteenth Street, Charlestown, MA 02129, USA.jcohen@nmr.mgh.harvard.edu. .

the study of patterns of cell morphology, size and density (Brodmann, 1909; Economo and Koskinas, 1925) while myeloarchitectonics refers to the study of patterns of myelinated fibers (including size, density orientation, and myelination) (Flechsig, 1920; Vogt, 1910).

Magnetic resonance imaging (MRI) has shown great potential for retrieving features of tissue microarchitecture in the living brain. Previous works demonstrated associations between myelin concentration and T_1-weighted (Barbier et al., 2002; Clark et al., 1992) and T_1-weighted/T_2-weighted (Glasser and Van Essen, 2011) signals. Quantitative relaxometry measures have been shown to reflect myelin and iron content (Duyn et al., 2007; Eickhoff et al., 2005; Haacke et al., 2005); for example, previous in vivo studies at 3 T reported shorter T_1 in the visual cortex (Fischl et al., 2004; Sigalovsky et al., 2006) and shorter T_2-weighted signal in the primary motor (Dinçer et al., 2010; Kamada et al., 2008; Kim et al., 2009) and auditory (Yoshiura et al., 2000) cortices. Identification of cortical lamination structure has also been demonstrated using ultra-high resolution MRI measures (Barazany and Assaf, 2011; Chen et al., 2011; Walters et al., 2003).

Ultra-high field MRI (≥7 T) enables higher spatial resolution and provides higher contrast on T_2*-weighted imaging, resulting in greater sensitivity to depict patterns of tissue microarchitecture and myelin density (Bock et al., 2009, 2011; Duyn et al., 2007; Fukunaga et al., 2010; Sati et al., 2012). Recently, we mapped T_2*-weighted signal from 7 T data using a surface-based analysis technique (Cohen-Adad et al., 2011). Cortical mapping of MRI signal has previously been proposed as a means to study anatomical features in the gray matter cortex (Fischl et al., 2004; Glasser and Van Essen, 2011; Rebmann and Butman, 2003; Sigalovsky et al., 2006; Weiss et al., 2011). Surface rendering allows the robust visualization of MRI measurements across the entire cortex and enables the calculation of spatial statistics at a population scale. Being able to co-register cortical maps of structural and functional MRI data with probabilistic cytoarchitectonic maps in a common template will be of tremendous help for pursuing the parcellation of the cortex into microstructural and functional units in the living human brain (Geyer et al., 2011; Roland and Zilles, 1994). While efforts have been made to characterize *ex vivo* anatomical features of the cortex from 7 T data (Augustinack et al., 2005; Duyn et al., 2007; Fukunaga et al., 2010) and to compute voxel-wise T_2* values over the cortex (Peters et al., 2007), no study has provided cortical mapping of T_2* over the entire human cortex at 7 T.

The development of ultra-high field MRI has also raised interests about the dependence of T_2* on the orientation of myelinated fibers with respect to the main magnetic field, B_0 (Bender and Klose, 2010; Cherubini et al., 2009; Denk et al., 2011; Lee et al., 2010b; Liu, 2010; Sati et al., 2012; Schäfer et al., 2009b; Wiggins et al., 2008). This dependence is thought to arise from highly coherent and anisotropic structure of the myelin sheath in the white matter (Lee et al., 2011; Liu, 2010; Sati et al., 2012). These observations led to the recent development of susceptibility tensor imaging (Liu, 2010), which provides information on the orientation of white matter fibers based on the anisotropic effect of fibers on local susceptibility. Given that some fibers in the gray matter are myelinated and that the cortical gray matter has been shown to exhibit detectible anisotropy in diffusion tensor imaging measurements (Miller et al., 2011), we can ask whether such B_0 orientation dependency also exists in the cortex.

The aims of this study were: (*i*) to acquire high-resolution multi-echo measurements at 7 T in order to map T_2* over the entire cortex of healthy individuals using a surface-based analysis; (*ii*) to test the presence of a dependency between T_2* and the orientation of the cortical surface relative to B_0, and to assess whether this dependency underlies patterns of cyto- and myeloarchitectural organization of the human cortex.

Material and methods

Acquisition

Healthy subjects (N=8, age=41+/−8 years) were recruited. General exclusion criteria were significant medical, psychiatric, or neurologic history. The Institutional Review Board of the Massachusetts General Hospital approved all experimental procedures of the study, and written informed consent was obtained from each subject.

Subjects were scanned with a 7 T whole-body scanner (Siemens Healthcare, Erlangen, Germany) using an AC84 head gradient set and a custom-built 32-channel array coil (Keil et al., 2010). At the beginning of the session, multiple B_0 shimming was performed to minimize susceptibility effects. A transmit voltage map was acquired ('actual flip angle image' method) to manually set the voltage that produced a desired flip angle at the center of the brain. A multiecho 2D FLASH T_2*-weighted spoiled gradient-echo pulse sequence was run with the following parameter values: two axial slabs covering the supratentorial brain, TR=2020 ms, TE=6.34+3.2n [n=1,…,12], in-plane resolution = 0.33×0.33 mm^2, 1 mm slice thickness (25% gap), 40 slices, matrix = 576×504, BW = 335 Hz/pixel. For registration purposes a T_1-weighted MPRAGE was acquired with parameter values: TR/TI/TE = 2600/1100/3.26 ms, 0.60×0.60×1.5 mm^3.

Subjects were also scanned at 3 T (Tim Trio, Siemens Healthcare) using the vendor-supplied 32-channel coil. A multi-echo MPRAGE (van der Kouwe et al., 2008) was acquired for surface reconstruction and cortical thickness measurements. Parameter values were: TR/TI = 2530/1200 ms, TE = [1.7, 3.6, 5.4, 7.3] ms, flip angle=7°, FOV = 230×230 mm^2, resolution = 0.9×0.9×0.9 mm^3, bandwidth = 651 Hz/pixel.

Processing

Correction for background field gradients—Despite careful B_0 shimming, some inhomogeneities remained, especially in lower brain regions and in regions of air/tissue interface (*e.g.*, close to the sinuses). These inhomogeneities induced background field gradients within each voxel, resulting in shorter T_2* decay (Yablonskiy and Haacke, 1994) and therefore underestimation of T_2* (Fernández-Seara and Wehrli, 2000; Peters et al., 2007). When anisotropic voxel is used, the slice-select direction (Z) is particularly sensitive to these background gradients (Frahm et al., 1988). This effect can be compensated by correcting each T_2*-weighted signal according to the formulation introduced in Yablonskiy and Haacke (1994), which expresses the signal $S(T_E)$ in the presence of background field gradient:

$$S(T_E) = S_0 \cdot \exp\left(\frac{-T_E}{T_2^*}\right) \cdot \left|\operatorname{sinc}\left(\frac{\gamma \cdot G \cdot \Delta z \cdot T_E}{2}\right)\right| \quad (1)$$

where S_0 is the signal strength at T_E=0, γ is the Larmor frequency, G is the strength of a constant field gradient in the slice direction and Δz is the slice thickness. We corrected the signal $S(T_E)$ by first estimating the gradient frequency field along Z: $\Delta Bz = \gamma.G.\Delta z$ and then dividing the signal $S(T_E)$ by the sinc term in Eq. (1), as done in Fernández-Seara and Wehrli (2000) and Peters et al. (2007). Estimation of the gradient frequency field ΔBz was performed as follows: after unwrapping the phase evolution at each voxel, the resonance frequency was calculated by fitting the slope of the phase versus echo time T_E using a linear least-square approach. The frequency map was then downsampled by 2 and fitted using a 3D polynomial regression model (3rd order). The frequency gradient ΔBz was calculated analytically by deriving the polynomial expression along Z.

T_2* fitting—T_2* was estimated voxel-wise by fitting the corrected T_2*-weighted signal (S_{corr}) versus echo time (T_E) using a Levenberg–Marquardt nonlinear regression model (tolerance = 0.0001, max iterations = 20). The fitting equation was:

$$S_{\text{corr}}(T_E) = S_0 \cdot \exp\left(\frac{-T_E}{T_2^*}\right) \quad (2)$$

Parameters T_2* and S_0 were initialized from linear least square fitting of $\log(S_{\text{corr}})$ versus T_E. Voxels with poor goodness of fit from the nonlinear estimation were excluded from further analysis (adjusted R^2<0.8).

Correction for gradient non-linearities—T_2* data were corrected for gradient non-linearity using a 3D deformation field calculated from the specifications of the Siemens AC84 head gradient, and the image data was resampled using trilinear interpolation.

Surface-based analysis—Cortical surface models were reconstructed from 3 T image data using FreeSurfer (http://surfer.nmr.mgh.harvard.edu/). Each of the two 7 T FLASH slabs was registered to the 3 T surface using a boundary-based registration technique (Greve and Fischl, 2009) with 9 degrees of freedom. The registration to the surface was achieved using the average of the first 4 echoes (6.34–15.94 ms), empirically found to be an acceptable compromise between SNR, white/gray matter contrast, and through-plane susceptibility artifacts. Registered slabs were then concatenated using FreeSurfer tools. For more details on the registration, the reader is referred to Cohen-Adad et al. (2011). T_2* was sampled along the midline between the pial and the white matter surface (50% depth) across the entire cortical hemisphere. Each individual T_2* map was normalized to the 'fsaverage' template surface available in FreeSurfer, then averaged across subjects and smoothed along the surface using a 3 mm FWHM Gaussian kernel. To identify regions of lower/higher T_2*, one-sample Student's *t*-test was performed on a vertex-by-vertex basis between the T_2* distribution (across subjects) and the median T_2* (across the cortex). Maps of $-\log(p)$ were generated (threshold at $p = 0.0001$ with FDR correction). To assess inter-hemispheric differences in T_2*, two-sample Student's *t*-test was performed in each sub-region of the cortex defined by the PALS-B12 Brodmann atlas available in FreeSurfer (Van Essen, 2005).

Cortical thickness was estimated for each subject based on the 3 T multi-echo MPRAGE using FreeSurfer (Fischl and Dale, 2000). The resulting thickness map was spatially normalized to the fsaverage template and then averaged across subjects for comparison with the T_2* maps.

B_0 orientation dependence—The effect of B_0 orientation on T_2* contrast was investigated on the basis of the radially and tangentially oriented fibers penetrating into the cortex and their potential effect on T_2*. Instead of using diffusion tensor information to relate orientation of B_0 and orientation of fiber bundles (Bender and Klose, 2010; Cherubini et al., 2009; Denk et al., 2011; Lee et al., 2011), we related the orientation of B_0 to the vector normal to the cortical surface (Fig. 1). To probe the existence of any B_0 orientation dependence, it was necessary to sample the tissue at various orientations within the bore. Here, instead of rotating the head of participants as done previously (Bender and Klose, 2010; Wiggins et al., 2008), we took advantage of the convoluted nature of the human cortical folding pattern to obtain a wide range of angles between B_0 and any intracortical fibers that are consistently aligned with the direction of the cortical surface (*i.e.*, radial or tangential). The angle θ_z between the main B_0 field and the vector normal to the mid surface was computed on a vertex-by-vertex basis. R_2* (inverse of T_2*) was then plotted against $\theta_z \in [0, \pi/2)$ and a regression was conducted within each region of the PALS-B12 Brodmann

atlas. The rationale for fitting the $R_2^*(\theta_z)$ data within Brodmann areas is that we can expect the local cyto/myeloarchitecture, which varies across the Brodmann areas, to drive the orientation dependence. The fitting equation is:

$$R_2^* = c_0 + c_1 \cdot \sin(2\theta_z + \varphi_0) \quad (3)$$

where c_0 represents the background portion of R_2^* that is not affected by B_0 orientation, c_1 represents the portion of R_2^* that does depend on B_0 orientation, and φ_0 is a phase offset term. This equation is derived from the model used by Lee et al. (2011) without the suggested $\sin(4\theta_z)$ term (*i.e.*, Eq. (3) corresponds to the *isotropic susceptibility* model). The reason for not including the $4\theta_z$ dependence was that susceptibility anisotropy (Lee et al., 2010b; Liu, 2010) has not been assessed in the gray matter. Another argument for choosing the Lee model is that, here, no assumption could be made on the orientation of the fibers with respect to B_0, therefore a phase parameter was required in the sinusoidal term (*e.g.*, to account for tangential versus radial fibers). Fitting was achieved in Matlab (The MathWorks, Inc., USA) using robust non-linear least squares fitting (bisquare weights method). Confidence bounds at 95% were calculated. The dependency of T_2^* toward B_0 orientation was assessed by the $|c_1|$ parameter, which scales the sinusoidal term in Eq. (3). Variation of R_2^* was computed as $\Delta R_2^* = 2|c_1|$.

Results

T_2^*-weighted data were successfully acquired and T_2^* estimated in all subjects ($N = 8$). Fig. 2 shows T_2^*-weighted data with the fitted values and the adjusted R^2 statistics (capturing the goodness-of-fit of the T_2^* model) in a representative subject.

The mean T_2^* over the cortex of all individuals was 32.20+/−1.35 ms (this average does not include the medial wall). Fig. 3A shows the average T_2^* mapped on the inflated surface. Regions with lower T_2^* are noticeable in the primary sensorimotor, occipital and temporal cortices. The 'strip' pattern of lower T_2^* in the sensorimotor region is centered along the central sulcus and extends across the pre- and post-central gyri. Missing or low T_2^* values located in the lower brain are due to poor coverage or through-slice susceptibility artifacts caused by large B_0-inhomogeneities.Fig. 3B shows results of the one-sample Student's *t*-test that assessed regional T_2^* differences compared to the T_2^* median across the cortex (threshold at $p<0.0001$ with correction for false discovery rate, FDR). As observed on the T_2^* map, lower T_2^* was detected in the primary sensorimotor ("1"), visual ("2") and auditory areas ("3"). Conversely, higher T_2^* was detected in the superior and middle frontal sulci ("4") and in the anterior and posterior cingulate ("5").

Fig. 4 shows the left lateral view of the mean T_2^* map with an overlay of the Brodmann areas predicted from the PALS-B12 atlas, the cortical thickness map computed from all subjects and the curvature map representing distribution of sulci and gyri. 'Strips' of lower T_2^* are noticeable on both sides of the central sulcus (indicated by the arrow) and correspond to a relatively large cortical thickness (2.5–3 mm). Conversely, the posterior bank of the central sulcus (area 3b/1), which has thinner cortex (1.5–2 mm), is associated with slightly higher T_2^*, which could result from partial volume effects with the cerebrospinal fluid (CSF). A measure of spatial correlation was computed between the T_2^* map and the cortical thickness map using the Spearman's coefficient, yielding $\rho = 0.0046$ (degrees of freedom = 275,929). Distribution of T_2^* resembles subdivisions of the Brodmann areas, with homogeneous regions of lower T_2^* in areas such as BA1 (primary somatosensory cortex), BA4 (primary motor cortex), BA19 (visual cortex) and BA42 (auditory association cortex). The bar graph shows T_2^* values averaged across subjects for each hemisphere. Most areas show fairly good reproducibility across hemispheres, however

significant differences were detected in areas BA22, BA37 ($p<0.05$) and BA42 ($p<0.005$). Significantly lower T_2* in the left hemisphere of the latter area (BA42) is of particular interest as it is in accordance with previous observations based on quantitative T_1 mapping (Sigalovsky et al., 2006) and will be further discussed.

Fig. 5A shows plots of $R_2^*(\theta_z)$ in two regions of the cortex defined by the PALS-B12 atlas (BA2 and BA4). These plots result from a concatenation of data from both hemispheres and all subjects ($N=8$). Variation of R_2*, expressed as $\Delta R_2^* = 2|c_1|$, was 0.48 Hz in BA2 and 4.10 Hz in BA4. This result suggests greater orientation dependence in BA4 compared to BA2 (by a factor 8.5). Fig. 5B shows a map of ΔR_2^* across 29 regions of the PALS-B12. Quantitative values for all regions are also displayed as a bar graph (error bars represent the 95% confidence bounds of the fit). ΔR_2^* ranges between 0 and 4.1 Hz. Highest ΔR_2^* values were detected in BA4, BA3 (primary somatosensory cortex), BA17 (V1, primary visual cortex), BA42 (auditory association cortex), BA44/45 (Broca's area) and particularly low ΔR_2^* was observed in BA2. Fig. 5C shows independent estimates of ΔR_2^* in each hemisphere of the cortex. Important inter-hemispheric differences were observed in BA2-3, BA7, BA9-11, BA18-19, BA23, BA42 and BA45-47 (ratio >2).

Discussion

T_2* was estimated in the cerebral cortex *in vivo* in healthy individuals from multi-echo measurements at 7 T and mapped into a common surface space. Lower T_2* was detected in some regions of the cortex, such as in the sensorimotor, visual and auditory cortices. B_0 orientation dependence of T_2* was detected in the cortex, shedding light into the potential use of this contrast for studying myeloarchitecture.

Origin of T_2* contrast

T_2* contrast in the cortex has been associated with non-heme iron stored in ferritin (Fukunaga et al., 2010; Haacke et al., 2005). Given the co-localization of iron and myelinated fibers, the presence of myelin also correlates with T_2* contrast (Connor et al., 1990). Water trapped in myelin has low T_2 relaxation time (~20 ms at 3 T) as opposed to the water within intra/extracellular compartments (~80 ms at 3 T), which is another cause for shorter T_2* in the presence of myelin (Du et al., 2007). T_2* can also be modulated by the local concentration of deoxyhemoglobin in venous blood (Duyn et al., 2007; Haacke et al., 2005) and by calcium concentration–a diamagnetic ion present at synaptic sites (Marques et al., 2009). For more information on the origin of the T_2* contrast, the reader is referred to references (Fukunaga et al., 2010; Haacke et al., 2005).

T_2* variations in the cortex

The averaged T_2* in the cortex was 32.20+/−1.35 ms(mean+/−SD). In comparison, Peters et al. (2007) found 33.2+/−1.3 ms. Although relatively small, this discrepancy might come from the possibly different regions of interest.

Lower T_2* was notably detected in BA1 (primary somatosensory cortex), BA4 (primary motor cortex), BA19 (visual cortex) and BA42 (auditory association cortex), relative to the rest of the cortex. Similar spatial patterns were also observed in the marmoset (Bock et al., 2011) and in humans using quantitative T_1 (Fischl et al., 2004; Geyer et al., 2011; Weiss et al., 2011) and measurements of the ratio between T_1- and T_2-weighted images (Glasser and Van Essen, 2011) and are likely due to an increase of myelin density in these regions.

The 'strip' pattern in the motor-somatosensory area has previously been reported in humans from T_2-weighted measurements at 3 T (Dinçer et al., 2010; Duyn et al., 2007; Kamada et al., 2008; Kim et al., 2009), from quantitative T_1 measurements (Fischl et al., 2004; Geyer et

al., 2011; Weiss et al., 2011) and from T_1w/T_2w signal (Glasser and Van Essen, 2011). In the latter study, areas 4 and 3b were found to be the most myelinated in comparison with areas 1 and 2. This is in agreement with our results that show shorter T_2^* in areas 3 and 4 versus area 2. T_2^* shortening is likely due to the higher myelin and iron content in cortical layers III to VI (Duyn et al., 2007; Ogg et al., 1999).

Lower T_2^* in the primary visual cortex (V1) has previously been reported at 3 T (Wansapura et al., 1999) and 7 T (Duyn et al., 2007). Plausible causes for lower T_2^* in V1 include the presence of high myelin content at cell layer IV (at the line of Gennari), also observed *ex vivo* (Fukunaga et al., 2010; Hinds et al., 2008; Walters et al., 2003) and *in vivo* using T_1-weighted (Barbier et al., 2002; Bridge et al., 2005; Clare et al., 2001; Clark et al., 1992; Eickhoff et al., 2005), T_2-weighted (Carmichael et al., 2006; Trampel et al., 2011), T_2^*-weighted (Duyn et al., 2007) and quantitative T_1 (Fischl et al., 2004; Sigalovsky et al., 2006; Turner et al., 2008) measurements. Given that V1 has relatively thin cortex, it is possible that partial voluming with the CSF was higher in this region.

Lower T_2^* in the auditory associative cortex (BA42) could also be explained by greater myelin density, in accordance with a previous study reporting lower T_1 (Sigalovsky et al., 2006) and lower T_2-weighted signal (Yoshiura et al., 2000) in the Heschl's gyrus. In addition, T_2^* in BA42 of the left hemisphere was significantly lower than that in the right hemisphere ($p<0.005$). In the same article by Sigalowsky et al., inter-hemispheric difference in the auditory cortex was also detected, with lower T_1 in the left hemisphere. Lower T_1 and lower T_2^* are both consistent with greater gray matter myelination in left auditory cortex. These observations are also supported by previous *ex vivo* data (Anderson et al., 1999; Buxhoeveden et al., 2001; Galuske et al., 2000; Hutsler and Gazzaniga, 1996; Seldon, 1981a, b, 1982) and suggest that higher myelination may be a substrate for the left hemisphere's specialized processing of speech, language, and rapid acoustic changes. The two other areas showing significant inter-hemispheric differences (BA22, BA37, $p<0.05$) are located in lower regions of the brain that show high susceptibility artifacts, therefore no conclusion could be drawn on the genuineness of this difference.

It is possible that the cellular organization (orientation, density) also contributed to the T_2^* singularities observed in some areas of the cortex, given the remarkable spatial correspondence of the T_2^* map with the Brodmann atlas (Van Essen, 2005), although at this point it is still difficult to disentangle cellular organization from iron and myelin contribution to the T_2^* contrast (Fukunaga et al., 2010). This ambiguity highlights the need to perform further measurements based on different biophysical properties, such as quantitative magnetization transfer (Levesque and Pike, 2009), diffusion tensor imaging (Basser and Pierpaoli, 1996) or myelin water mapping from T_2 relaxometry (MacKay et al., 2006). Each of these metrics shows high specificity toward myelin content, therefore combining them together into a common space using surface-based analysis could help studies of cortical parcellation and disentangle the effect of cytoversus myeloarchitecture in the generation of the T_2^* contrast.

Cortical thickness

A similar strip pattern along the central sulcus was observed when comparing the T_2^* map and the cortical thickness map. Notably, the posterior bank of the central sulcus, which has thinner cortex (1.5–2 mm), was associated with slightly higher T_2^*. Conversely, area V1 exhibited both thinner cortex and lower T_2^*. While some regions exhibiting low or high T_2^* corresponded to regions of thick or thin cortex, the two maps are largely independent. Spearman's coefficient showed low spatial correlation between the two maps ($\rho=0.0046$). Thus, we can conclude that the measured T_2^* is not simply reflecting cortical thickness differences (due to, *e.g.*, partial volume effects).

B_0 orientation dependence

The effect of the main magnetic field (B_0) orientation on T_2* contrast was investigated, in line with previous studies reporting B_0 dependence of T_2* magnitude and phase with respect to the orientation of fibers bundles in the white matter (Bender and Klose, 2010; Cherubini et al., 2009; Denk et al., 2011; Lee et al., 2010b; Liu, 2010; Sati et al., 2012; Schäfer et al., 2009b; Wiggins et al., 2008) or at the white/gray matter interface (Schäfer et al., 2009a). This dependence is thought to arise from highly coherent and anisotropic molecular structure of the phospholipid bilayer of the myelin sheath, which has been shown to exhibit susceptibility in vitro (Boroske and Helfrich, 1978; Scholz et al., 1984; Speyer et al., 1987). Here, given the limited amount of information on the orientation of fibers in the cortex, we explored this B_0 dependence by looking at the angle between the cortical surface and B_0. We assumed that fibers exhibit similar orientation relative to the cortical surface, within regions that are anatomically distinct on the basis of their cytoarchitecture (as defined by Brodmann areas). Our results show variable B_0 dependencies across the cortex, the highest dependency being in the primary motor cortex (BA4) where orientation-dependent variation of R_2* was 4.10 Hz (fitted using the isotropic model). In comparison, Lee et al. (2011) found ΔR_2*=6.44 Hz+/−0.15 in the corpus callosum at 7 T (fitted using the anisotropic model). Possible explanations for a lower ΔR_2* in our experiment are that fiber bundles in the corpus callosum are more dense than that in the cortex and exhibit higher coherency, therefore creating a greater bulk susceptibility, which in turn yields greater orientation dependence with respect to B_0. This argument is supported by the study of Sati et al., in which no significant change of R_2* was found in the gray matter cortex of marmosets imaged in sphinx and supine position, whereas strong dependence was observed in the optic radiation in the white matter (Sati et al., 2012). The discrepancy between our study and the study from Sati et al. suggests that subtle R_2* changes related to B_0 orientation may only be seen in the gray matter by multiple sampling of the angle between cortical fibers and B_0, combined with subsequent modeling of the R_2* dependency using cylindrical susceptibility perturbers (Lee et al., 2010a). Comparing our results with 3 T measurements in the *in vivo* white matter, Bender et al. found ΔR_2*=2.68 Hz (Bender and Klose, 2010) and Denk et al. found ΔR_2*=1.65 Hz (Denk et al., 2011). While these two studies looked at R_2* variation in white matter, the higher cortical ΔR_2* found here likely comes from the higher field strength (7 T versus 3 T). ΔR_2* estimated independently in each hemisphere seemed fairly reproducible in some areas, although important differences were observed in BA2-3, BA7, BA9-11, BA18-19, BA23, BA42 and BA45-47 (ratio >2 between left and right hemisphere). This variability can be accounted by the relatively low number and uneven distribution of θ_z values sampled in some areas; hence, reducing the number of θ_z values by a factor of two further reduced the robustness of the fit. For example, if in one Brodmann area we observe a cluster of θ_z values,the corresponding area in the other hemisphere may exhibit a different pattern of θ_z due to differences in the geometry of the folding patter, resulting in a different bias in the R_2* fit calculated for each hemisphere. Another source of inter-hemispheric variability is the presence of B_0 inhomogeneities in lower brain regions and close to the sinuses, which yielded unreliable estimate of R_2*. A third explanation is that the actual microstructure might be different in the two hemispheres of a given Brodmann area, as been shown, *e.g.*, in the auditory cortex (Sigalovsky et al., 2006).

Regions that were particularly affected by the orientation dependence were BA4 (primary motor cortex), BA3 (primary somatosensory cortex), BA17 (primary visual cortex V1), BA42 (auditory association cortex) and BA44/45 (Broca's area). Interestingly, those regions are also known to be heavily myelinated (Barbier et al., 2002; Duyn et al., 2007; Sigalovsky et al., 2006). In addition to myelin content, we might hypothesize that myelinated fibers are coherently oriented in these areas, hence yielding the orientation dependence reported in previous white matter studies. To verify this hypothesis, we compared our map of B_0

dependence (ΔR_2^*) with a map of fractional anisotropy (FA) generated from 1 mm isotropic diffusion tensor imaging (DTI) data acquired at 3 T in six other healthy subjects (McNab et al., 2011). FA is a measure of the anisotropy of water diffusion, and sometimes indicates the level of orientational coherence within a bundle of myelinated fibers (Beaulieu, 2002). FA was mapped along the mid-surface of each individual, normalized to the same fsaverage template and averaged across subjects. Fig. 6 shows the ΔR_2^* map and the FA map with an overlay of the PALS-B12 Brodmann areas. Higher ΔR_2^* (*i.e.*, higher B_0 dependence) is associated with higher FA in BA4, and lower B_0 dependence is associated with lower FA in BA2. Note that some regions show high FA without systematic higher B_0 dependence. This could be explained by the methodology that was used here: FA was estimated voxelwise and then mapped on the surface, whereas ΔR_2^* was estimated for the whole Brodmann area (including thousands of vertices). Hence, it is possible that within each vertex fibers showed high coherence and low amount of crossings (hence high FA), but within some Brodmann areas the orientation of fibers may have been different, therefore yielding low ΔR_2^*.

Effect of blood vessels

Radially penetrating vessels may have influenced T_2^* dependence with respect to B_0 (Petridou et al., 2010). This effect may have been emphasized due to the anisotropic shape of our voxel size (Denk et al., 2011). However, the venous blood volume fraction is only about 3% in the human cortex (Buxton et al., 2004), suggesting that the contribution of blood vessels to the B_0 dependency is marginal (Lee et al., 2010a; Petridou et al., 2010). Hence, we think that blood vessel only marginally contributed to the B_0 dependence in the cortex, and that the primary reason for this dependence was myeloarchitecture features. Future studies should be conducted to investigate the contribution of blood vessels to the B_0 dependence, *e.g.*, studies employing carbogen – a mixture of carbon dioxide and oxygen gas that increases blood flow and therefore reduces deoxyhemoglobin concentration.

Limitations and future studies

We used anisotropic voxels in order to acquire the entire cortex in a reasonable scan time while maintaining high in-plane resolution (300×300 μm). Anisotropic voxels suffer from more severe partial volume effects in the through-plane direction. Thus cortical regions parallel to the image slice are worst affected and may also show a larger effect of coherently oriented cortical veins. In future, EPI-based multi-echo measurements (Zwanenburg et al., 2011) may accelerate acquisition enough to allow use of more isotropic voxels, provided that distortion correction is applied as required.

T_2^* mapping of the cortex may be useful in the diagnosis of disease, as well as understanding pathogenesis, disease progression and the monitoring of treatment. It may help to quantify changes in iron concentration related to healthy aging (Hirai et al., 1996) or to pathologies such as Alzheimer Disease (Benveniste et al., 1999) and multiple sclerosis (Craelius et al., 1982). The good spatial correspondence between our T_2^* map, the B_0 dependence map, Brodmann map and regions of high myelin content suggests that T_2^* and B_0 dependence mapping could provide useful information for studying the cytoarchitecture (Brodmann, 1909; Economo and Koskinas, 1925) and myeloarchitecture (Flechsig, 1920; Geyer et al., 2011) in thecortex, and guiding the development of cortical atlasing and parcellation methods (Eickhoff et al., 2005; Van Essen, 2005; Zilles, 2004).

One specific application of B_0 dependence analysis is the exploration of fiber orientation within the cortex, previously described using DTI (Anwander et al., 2010; McNab et al., 2011). While B_0 orientation dependence in the white matter can potentially help to study features of axonal organization, we believe that studying B_0 orientation dependence in the

gray matter potentially has some relevance, as it might reveal new features of cortical fiber distribution and monitor re-myelination in diseases (*e.g.*, multiple sclerosis).

Apart from these possible applications, B_0 dependence in the cortex has some impact in relaxometry studies, where T_2* is used as a biomarker or to develop parcellation methods. As demonstrated here, T_2* is influenced by the angle between cortical fibers and B_0 orientation. Hence, it is possible that spurious apparent boundaries and/or apparent change in tissue contrast within a homogeneous region (on the basis of its cellular organization) would result from a pure B_0 orientation dependence effect. For instance, the recent study of Sati et al. showed drastic R_2* change within the optic radiation in marmosets images in supine versus sphinx position (Sati et al., 2012), and other studies showed changes in the human pyramidal tract (Bender and Klose, 2010) and corpus callosum (Wiggins et al., 2008) depending on the orientation of the head. Future studies should aim at developing methods to correct for this orientation dependence, allowing to estimate a more intrinsic T_2* value (*i.e.*, not depending on subject's orientation in the scanner). One possibility would be to estimate the angle between fiber bundles and B_0 from DTI measurements, and then derive a spatial map of B_0 dependence associated with a correcting factor to be applied to T_2* measurements. This correcting factor could be calculated from models of field perturbations (Schäfer et al., 2009a; Wharton et al., 2009; Yablonskiy and Haacke, 1994). Although more challenging, robust and precise *in vivo* measurements of fiber bundles orientation in the cortex were shown to be feasible thanks to the use of highly parallelized phased-array receive coils (McNab et al., 2011) and increased magnetic field strength (Heidemann et al., 2010).

Acknowledgments

We thank Drs. Doug Greve, Bruce Fischl and Kawin Setsompop for helpful discussions and Dr. Boris Keil for helping with the 7 T coil. This work was supported by the National Multiple Sclerosis Society [FG 1892A1/1 to J.C-A], [Grant 4281-RG-A-1 to C.M.], by the National Center for Research Resources [P41-RR14075, and the NCRR BIRN Morphometric, Project BIRN002, U24 RR021382] and by the NIH [Human Connectome Project, U01MH093765].

References

Anderson B, Southern BD, Powers RE. Anatomic asymmetries of the posterior superior temporal lobes: a postmortem study. Neuropsychiatry Neuropsychol Behav. Neurol. 1999; 12:247–254. [PubMed: 10527109]

Anwander, A.; Pampel, A.; Knösche, TR. In vivo measurement of cortical anisotropy by diffusion-weighted imaging correlates with cortex type. Proceedings of the 18th Annual Meeting of ISMRM; Stockholm, Sweden. 2010. p. 109

Augustinack JC, van der Kouwe AJW, Blackwell ML, Salat DH, Wiggins CJ, Frosch MP, Wiggins GC, Potthast A, Wald LL, Fischl BR. Detection of entorhinal layer II using 7 Tesla [corrected] magnetic resonance imaging. Ann. Neurol. 2005; 57:489–494. [PubMed: 15786476]

Barazany D, Assaf Y. Visualization of cortical lamination patterns with magnetic resonance imaging. Cereb. Cortex. 2011 doi:10.1093/cercor/bhr277.

Barbier EL, Marrett S, Danek A, Vortmeyer A, van Gelderen P, Duyn J, Bandettini P, Grafman J, Koretsky AP. Imaging cortical anatomy by high-resolution MR at 3.0 T: detection of the stripe of Gennari in visual area 17. Magn. Reson. Med. 2002; 48:735–738. [PubMed: 12353293]

Basser PJ, Pierpaoli C. Microstructural and physiological features of tissues elucidated by quantitative-diffusion-tensor MRI. J. Magn. Reson. B. 1996; 111:209–219. [PubMed: 8661285]

Beaulieu C. The basis of anisotropic water diffusion in the nervous system – a technical review. NMR Biomed. 2002; 15:435–455. [PubMed: 12489094]

Bender B, Klose U. The in vivo influence of white matter fiber orientation towards B(0) on T2* in the human brain. NMR Biomed. 2010; 23:1071–1076. [PubMed: 20665897]

Benveniste H, Einstein G, Kim KR, Hulette C, Johnson GA. Detection of neuritic plaques in Alzheimer's disease by magnetic resonance microscopy. Proc. Natl. Acad. Sci. U. S. A. 1999; 96:14079–14084. [PubMed: 10570201]

Bock NA, Kocharyan A, Liu JV, Silva AC. Visualizing the entire cortical myelination pattern in marmosets with magnetic resonance imaging. J. Neurosci. Methods. 2009; 185:15–22. [PubMed: 19737577]

Bock NA, Hashim E, Kocharyan A, Silva AC. Visualizing myeloarchitecture with magnetic resonance imaging in primates. Ann. N. Y. Acad. Sci. 2011; 1225(Suppl. 1):E171–E181. [PubMed: 21599695]

Boroske E, Helfrich W. Magnetic anisotropy of egg lecithin membranes. Biophys. J. 1978; 24:863–868. [PubMed: 367463]

Bridge H, Clare S, Jenkinson M, Jezzard P, Parker AJ, Matthews PM. Independent anatomical and functional measures of the V1/V2 boundary in human visual cortex. J. Vis. 2005; 5:93–102. [PubMed: 15831070]

Brodmann, K. Vergleichende Lokalisationslehre der Grosshirnrinde in ihren Prinzipien dargestellt auf Grund des Zellenbaues. Barth, Leipzig: 1909.

Buxhoeveden DP, Switala AE, Litaker M, Roy E, Casanova MF. Lateralization of minicolumns in human planum temporale is absent in nonhuman primate cortex. Brain Behav. Evol. 2001; 57:349–358. [PubMed: 11713389]

Buxton RB, Uludag K, Dubowitz DJ, Liu TT. Modeling the hemodynamic response to brain activation. NeuroImage. 2004; 23(Suppl. 1):S220–S233. [PubMed: 15501093]

Carmichael DW, Thomas DL, De Vita E, Fernández-Seara MA, Chhina N, Cooper M, Sunderland C, Randell C, Turner R, Ordidge RJ. Improving whole brain structural MRI at 4.7 Tesla using 4 irregularly shaped receiver coils. NeuroImage. 2006; 32:1176–1184. [PubMed: 16806980]

Chen G, Wang F, Gore JC, Roe AW. Identification of cortical lamination in awake monkeys by high resolution magnetic resonance imaging. NeuroImage. 2011 doi:10.1016/j.neuroimage.2011.10.079.

Cherubini A, Péran P, Hagberg GE, Varsi AE, Luccichenti G, Caltagirone C, Sabatini U, Spalletta G. Characterization of white matter fiber bundles with T2* relaxometry and diffusion tensor imaging. Magn. Reson. Med. 2009; 61:1066–1072. [PubMed: 19253372]

Clare, S.; Jezzard, P.; Matthews, PM. Identification of the myelinated layers in striate cortex on high resolution MRI at 3 Tesla. Proceedings of the 10th Annual Meeting of ISMRM; Honolulu, USA. 2001. p. 1465

Clark VP, Courchesne E, Grafe M. In vivo myeloarchitectonic analysis of human striate and extrastriate cortex using magnetic resonance imaging. Cereb. Cortex. 1992; 2:417–424. [PubMed: 1422094]

Cohen-Adad J, Benner T, Greve DN, Kinkel RP, Radding A, Fischl B, Rosen BR, Mainero C. In vivo evidence of disseminated subpial T2* signal changes in multiple sclerosis at 7 T: a surface-based analysis. NeuroImage. 2011; 57:55–62. [PubMed: 21511042]

Connor JR, Menzies SL, St Martin SM, Mufson EJ. Cellular distribution of transferrin, ferritin, and iron in normal and aged human brains. J. Neurosci. Res. 1990; 27:595–611. [PubMed: 2079720]

Craelius W, Migdal MW, Luessenhop CP, Sugar A, Mihalakis I. Iron deposits surrounding multiple sclerosis plaques. Arch. Pathol. Lab. Med. 1982; 106:397–399. [PubMed: 6896630]

Denk C, Hernandez Torres E, Mackay A, Rauscher A. The influence of white matter fibre orientation on MR signal phase and decay. NMR Biomed. 2011; 24:246–252. [PubMed: 21404336]

Dinçer A, Özyurt O, Erzen C, Pamir MN. Identification of the primary motor cortex: value of T2 echo-planar imaging, diffusion-weighted imaging and quantitative apparent diffusion coefficient measurement at 3 T. Eur. Radiol. 2010; 20:931–940. [PubMed: 19890649]

Du YP, Chu R, Hwang D, Brown MS, Kleinschmidt-Demasters BK, Singel D, Simon JH. Fast multislice mapping of the myelin water fraction using multicompartment analysis of T2* decay at 3 T: a preliminary postmortem study. Magn. Reson. Med. 2007; 58:865–870. [PubMed: 17969125]

Duyn JH, van Gelderen P, Li TQ, de Zwart JA, Koretsky AP, Fukunaga M. High-field MRI of brain cortical substructure based on signal phase. Proc. Natl. Acad. Sci. U. S. A. 2007; 104:11796–11801. [PubMed: 17586684]

Economo, C.; Koskinas, GN. Die Cytoarchitektonik der Hirnrinde des erwachsenen Menschen. 1925.

Eickhoff S, Walters NB, Schleicher A, Kril J, Egan GF, Zilles K, Watson JDG, Amunts K. High-resolution MRI reflects myeloarchitecture and cytoarchitecture of human cerebral cortex. Hum. Brain Mapp. 2005; 24:206–215. [PubMed: 15543596]

Fernández-Seara MA, Wehrli FW. Postprocessing technique to correct for background gradients in image-based R*(2) measurements. Magn. Reson. Med. 2000; 44:358–366. [PubMed: 10975885]

Fischl B, Dale AM. Measuring the thickness of the human cerebral cortex from magnetic resonance images. Proc. Natl. Acad. Sci. U. S. A. 2000; 97:11050–11055. [PubMed: 10984517]

Fischl B, Salat DH, van der Kouwe AJW, Makris N, Ségonne F, Quinn BT, Dale AM. Sequence-independent segmentation of magnetic resonance images. NeuroImage. 2004; 23(Suppl. 1):S69–S84. [PubMed: 15501102]

Flechsig, P. Anatomie des menschichen Gehirns und Ruckenmarks auf Myelogenetischer Grundlage. 1920.

Frahm J, Merboldt KD, Hänicke W. Direct FLASH MR imaging of magnetic field inhomogeneities by gradient compensation. Magn. Reson. Med. 1988; 6:474–480. [PubMed: 3380007]

Fukunaga M, Li T-Q, Van Gelderen P, De Zwart JA, Shmueli K, Yao B, Lee J, Maric D, Aronova MA, Zhang G, Leapman RD, Schenck JF, Merkle H, Duyn JH. Layer-specific variation of iron content in cerebral cortex as a source of MRI contrast. Proc. Natl. Acad. Sci. U. S. A. 2010; 107:3834–3839. [PubMed: 20133720]

Galuske RA, Schlote W, Bratzke H, Singer W. Interhemispheric asymmetries of the modular structure in human temporal cortex. Science. 2000; 289:1946–1949. [PubMed: 10988077]

Geyer S, Weiss M, Reimann K, Lohmann G, Turner R. Microstructural parcellation of the human cerebral cortex – from Brodmann's post-mortem map to in vivo mapping with high-field magnetic resonance imaging. Front. Hum. Neurosci. 2011; 5:19. [PubMed: 21373360]

Glasser MF, Van Essen DC. Mapping human cortical areas in vivo based on myelin content as revealed by t1- and t2-weighted MRI. J. Neurosci. 2011; 31:11597–11616. [PubMed: 21832190]

Greve DN, Fischl B. Accurate and robust brain image alignment using boundary-based registration. NeuroImage. 2009; 48:63–72. [PubMed: 19573611]

Haacke EM, Cheng NYC, House MJ, Liu Q, Neelavalli J, Ogg RJ, Khan A, Ayaz M, Kirsch W, Obenaus A. Imaging iron stores in the brain using magnetic resonance imaging. Magn. Reson. Imaging. 2005; 23:1–25. [PubMed: 15733784]

Heidemann RM, Porter DA, Anwander A, Feiweier T, Heberlein K, Knösche TR, Turner R. Diffusion imaging in humans at 7 T using readout-segmented EPI and GRAPPA. Magn. Reson. Med. 2010; 64:9–14. [PubMed: 20577977]

Hinds O, Polimeni JR, Rajendran N, Balasubramanian M, Wald LL, Augustinack JC, Wiggins G, Rosas HD, Fischl B, Schwartz EL. The intrinsic shape of human and macaque primary visual cortex. Cereb. Cortex. 2008; 18:2586–2595. [PubMed: 18308709]

Hirai T, Korogi Y, Sakamoto Y, Hamatake S, Ikushima I, Takahashi M. T2 shortening in the motor cortex: effect of aging and cerebrovascular diseases. Radiology. 1996; 199:799–803. [PubMed: 8638008]

Hutsler JJ, Gazzaniga MS. Acetylcholinesterase staining in human auditory and language cortices: regional variation of structural features. Cereb. Cortex. 1996; 6:260–270. [PubMed: 8670655]

Kamada K, Kakeda S, Ohnari N, Moriya J, Sato T, Korogi Y. Signal intensity of motor and sensory cortices on T2-weighted and FLAIR images: intraindividual comparison of 1.5 T and 3 T MRI. Eur. Radiol. 2008; 18:2949–2955. [PubMed: 18642001]

Keil, B.; Triantafyllou, C.; Hamm, M.; Wald, LL. Design optimization of a 32-channel head coil at 7 T. Proceedings of the 18th Annual Meeting of ISMRM; Stockholm, Sweden. 2010. p. 1493

Kim EY, Kim D-H, Chang J-H, Yoo E, Lee J-W, Park H-J. Triple-layer appearance of Brodmann area 4 at thin-section double inversion-recovery MR imaging. Radiology. 2009; 250:515–522. [PubMed: 19098226]

Lee J, Hirano Y, Fukunaga M, Silva AC, Duyn JH. On the contribution of deoxy-hemoglobin to MRI gray-white matter phase contrast at high field. NeuroImage. 2010a; 49:193–198. [PubMed: 19619663]

Lee J, Shmueli K, Fukunaga M, van Gelderen P, Merkle H, Silva AC, Duyn JH. Sensitivity of MRI resonance frequency to the orientation of brain tissue microstructure. Proc. Natl. Acad. Sci. U. S. A. 2010b; 107:5130–5135. [PubMed: 20202922]

Lee J, van Gelderen P, Kuo L-W, Merkle H, Silva AC, Duyn JH. T(2)*-based fiber orientation mapping. NeuroImage. 2011; 57:225–234. [PubMed: 21549203]

Levesque IR, Pike GB. Characterizing healthy and diseased white matter using quantitative magnetization transfer and multicomponent T(2) relaxometry: a unified view via a four-pool model. Magn. Reson. Med. 2009; 62:1487–1496. [PubMed: 19859946]

Liu C. Susceptibility tensor imaging. Magn. Reson. Med. 2010; 63:1471–1477. [PubMed: 20512849]

MacKay A, Laule C, Vavasour I, Bjarnason T, Kolind S, Mädler B. Insights into brain microstructure from the T2 distribution. Magn. Reson. Imaging. 2006; 24:515–525. [PubMed: 16677958]

Marques JP, Maddage R, Mlynarik V, Gruetter R. On the origin of the MR image phase contrast: an in vivo MR microscopy study of the rat brain at 14.1. T. NeuroImage. 2009; 46:345–352.

McNab, JA.; Polimeni, JR.; Wald, LL. Surface based analysis of diffusion orientation for identifying architectonic domains in the in vivo human cortex. Proceedings of the 19th Annual Meeting of ISMRM; Montreal, Canada. 2011. p. 412

Miller KL, Stagg CJ, Douaud G, Jbabdi S, Smith SM, Behrens TEJ, Jenkinson M, Chance SA, Esiri MM, Voets NL, Jenkinson N, Aziz TZ, Turner MR, JohansenBerg H, McNab JA. Diffusion imaging of whole, post-mortem human brains on a clinical MRI scanner. NeuroImage. 2011; 57:167–181. [PubMed: 21473920]

Ogg RJ, Langston JW, Haacke EM, Steen RG, Taylor JS. The correlation between phase shifts in gradient-echo MR images and regional brain iron concentration. Magn. Reson. Imaging. 1999; 17:1141–1148. [PubMed: 10499676]

Peters AM, Brookes MJ, Hoogenraad FG, Gowland PA, Francis ST, Morris PG, Bowtell R. T2* measurements in human brain at 1.5, 3 and 7 T. Magn. Reson. Imaging. 2007; 25:748–753. [PubMed: 17459640]

Petridou N, Wharton SJ, Lotfipour A, Gowland P, Bowtell R. Investigating the effect of blood susceptibility on phase contrast in the human brain. NeuroImage. 2010; 50:491–498. [PubMed: 20026280]

Rebmann, A.; Butman, JA. Heterogeneity of MR signal intensity mapped onto brain surface models. Proceedings of the 32nd Applied Imagery Pattern Recognition Workshop; 2003. p. 5

Roland PE, Zilles K. Brain atlases – a new research tool. Trends Neurosci. 1994; 17:458–467. [PubMed: 7531886]

Sati P, Silva AC, van Gelderen P, Gaitan MI, Wohler JE, Jacobson S, Duyn JH, Reich DS. In vivo quantification of T2* anisotropy in white matter fibers in marmoset monkeys. NeuroImage. 2012; 59:979–985. [PubMed: 21906687]

Schäfer, A.; Bowtell, R.; Turner, R. Orientation dependence of grey/white matter contrast in ultra high fields. Proceedings of the 17th Annual Meeting of ISMRM; Honolulu, USA. 2009a. p. 2921

Schäfer, A.; Wiggins, CJ.; Turner, R. Understanding the orientation dependent T2* contrast of the cingulum in ultra high fields. Proceedings of the 17th Annual Meeting of ISMRM; Honolulu, USA. 2009b. p. 956

Scholz F, Boroske E, Helfrich W. Magnetic anisotropy of lecithin membranes. A new anisotropy susceptometer. Biophys. J. 1984; 45:589–592.

Seldon HL. Structure of human auditory cortex. I. Cytoarchitectonics and dendritic distributions. Brain Res. 1981a; 229:277–294. [PubMed: 7306814]

Seldon HL. Structure of human auditory cortex. II. Axon distributions and morphological correlates of speech perception. Brain Res. 1981b; 229:295–310. [PubMed: 7306815]

Seldon HL. Structure of human auditory cortex. III. Statistical analysis of dendritic trees. Brain Res. 1982; 249:211–221.

Sigalovsky IS, Fischl B, Melcher JR. Mapping an intrinsic MR property of gray matter in auditory cortex of living humans: a possible marker for primary cortex and hemispheric differences. NeuroImage. 2006; 32:1524–1537. [PubMed: 16806989]

Speyer JB, Sripada PK, Das Gupta SK, Shipley GG, Griffin RG. Magnetic orientation of sphingomyelin – lecithin bilayers. Biophys. J. 1987; 51:687–691. [PubMed: 3580492]

Trampel R, Ott DVM, Turner R. Do the congenitally blind have a stria of Gennari? First intracortical insights in vivo. Cereb. Cortex. 2011; 21:2075–2081. [PubMed: 21310782]

Turner R, Oros-Peusquens A-M, Romanzetti S, Zilles K, Shah NJ. Optimised in vivo visualisation of cortical structures in the human brain at 3 T using IR-TSE. Magn. Reson. Imaging. 2008; 26:935–942. [PubMed: 18524522]

van der Kouwe AJ, Benner T, Salat DH, Fischl B. Brain morphometry with multiecho MPRAGE. NeuroImage. 2008; 40:559–569. [PubMed: 18242102]

Van Essen DC. A Population-Average, Landmark- and Surface-based (PALS) atlas of human cerebral cortex. NeuroImage. 2005; 28:635–662. [PubMed: 16172003]

Vogt O. Die myeloarchitektonische Felderung des menschlichen Stirnhirns. J. Psychol. Neurol. 1910; 15:221–238.

Walters NB, Egan GF, Kril JJ, Kean M, Waley P, Jenkinson M, Watson JDG. In vivo identification of human cortical areas using high-resolution MRI: an approach to cerebral structure – function correlation. Proc. Natl. Acad. Sci. U. S. A. 2003; 100:2981–2986. [PubMed: 12601170]

Wansapura JP, Holland SK, Dunn RS, Ball WS. NMR relaxation times in the human brain at 3.0. Tesla. J. Magn. Reson. Imaging. 1999; 9:531–538.

Weiss, M.; Geyer, S.; Lohmann, G.; Trampel, R.; Turner, R. Quantitative T1 mapping at 7 Tesla identifies primary functional areas in the living human brain. Proceedings of the 19th Annual Meeting of ISMRM; Montreal, Canada. 2011. p. 2360

Wharton, SJ.; Schäfer, A.; Bowtell, R. Susceptibility Mapping in the Human Brain at 3 and 7 T. 2009. p. 464

Wiggins, CJ.; Gudmundsdottir, V.; Le Bihan, D.; Lebon, V.; Chaumeil, M. Orientation dependence of white matter T2* contrast at 7 T: a direct demonstration. Proceedings of the 16th Annual Meeting of ISMRM; Toronto, Canada. 2008. p. 237

Yablonskiy DA, Haacke EM. Theory of NMR signal behavior in magnetically inhomogeneous tissues: the static dephasing regime. Magn. Reson. Med. 1994; 32:749–763. [PubMed: 7869897]

Yoshiura T, Higano S, Rubio A, Shrier DA, Kwok WE, Iwanaga S, Numaguchi Y. Heschl and superior temporal gyri: low signal intensity of the cortex on T2-weighted MR images of the normal brain. Radiology. 2000; 214:217–221. [PubMed: 10644127]

Zilles K. Architecture of the human cerebral cortex. Regional and laminar organization. The Human Nervous System. The Human Nervous System. Elsevier Academic, Amsterdam. 2004:997–1055.

Zwanenburg JJM, Versluis MJ, Luijten PR, Petridou N. Fast high resolution whole brain T2* weighted imaging using echo planar imaging at 7 T. NeuroImage. 2011; 56:1902–1907. [PubMed: 21440070]

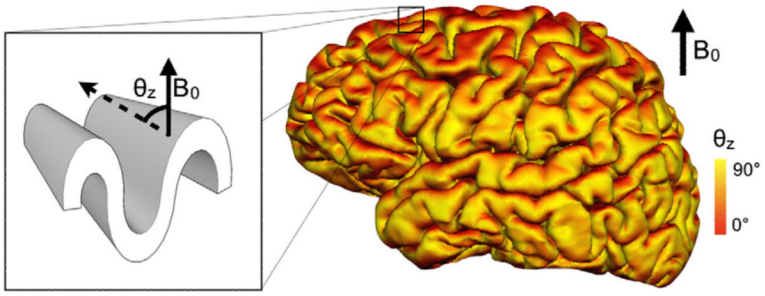

Fig. 1.

The effect of the main magnetic field (B_0) orientation on T_2* contrast was investigated on the basis of the radially and tangentially oriented fibers penetrating into the cortex. T_2* was sampled at 50% depth across the whole cortex, surface-smoothed with a 3 mm kernel and then plotted against θ_z (angle between the normal vector on the mid-surface and B_0). Here we used the surface of each individual (not the fsaverage surface). A map of θ_z is shown for one subject.

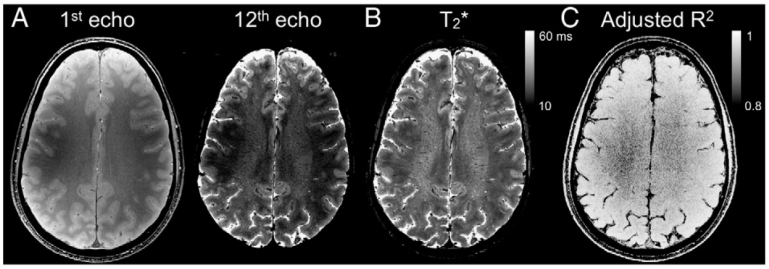

Fig. 2.

A. First (6 ms) and last echo (45 ms) of a FLASH T_2*-weighted image in a representative subject. B. T_2* map computed voxelwise from 12 echoes using least-squares fitting of the log of the data vs. echo time. C. Adjusted R^2 assessing the goodness of T_2* fit.

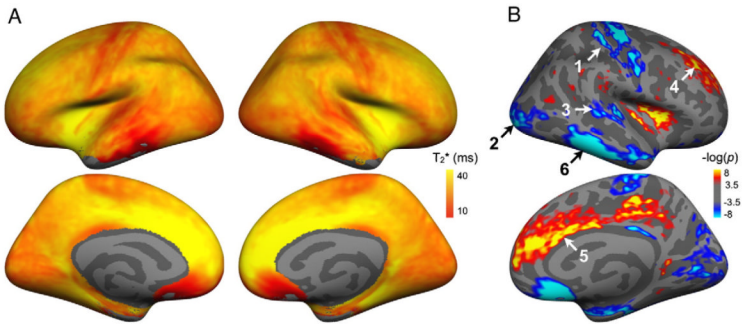

Fig. 3.

A. T_2* maps sampled at 50% depth, surface-smoothed with 5 mm kernel, normalized to the fsaverage template, averaged across subjects (N=8) and displayed on the inflated surface. B. Map of significant differences between T_2* in each vertex and the median value (p<0.0001, corrected for FDR). Lower T_2* is noticeable in the primary sensorimotor ("1"), visual ("2") and auditory areas ("3"). Higher T_2* is noticeable in the superior and middle frontal sulci ("4") and in the anterior and posterior cingulate ("5"). Missing or low T_2* values in the lower brain region ("6") are due to poor coverage or through-slice susceptibility artifacts.

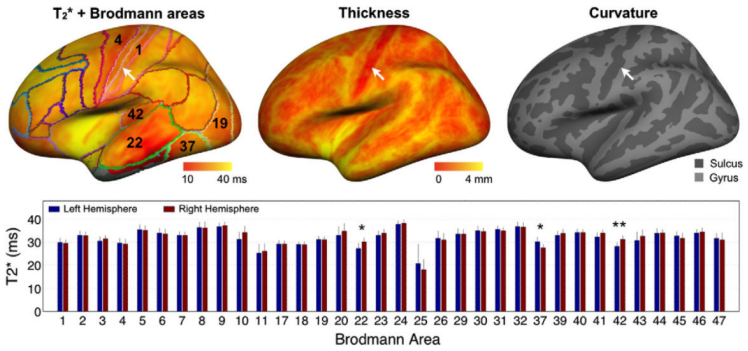

Fig. 4.

Lateral left view of the averaged T_2* map with an overlay of the PALS-B12 Brodmann atlas, which represents regions with specific cytoarchitectonics. The thickness map was computed from the 3 T MPRAGE data and averaged across subjects. The curvature map shows the distribution of gyri/sulci across the cortex. Strips of lower T_2* are noticeable on both sides of the central sulcus (arrows) and correspond to a larger cortical thickness. Distribution of T_2* resembles subdivisions of the Brodmann areas, with homogeneous regions of lower T_2* corresponding to *e.g.* BA1 (primary somatosensory), BA4 (primary motor), BA19 (visual) and BA42 (auditory). The bar graph shows T_2* values averaged across subjects for each hemisphere (error bars correspond to SD). Significant differences between hemispheres were assessed using a Student's *t*-test and significance levels are displayed as *: $p<0.05$; **: $p<0.005$.

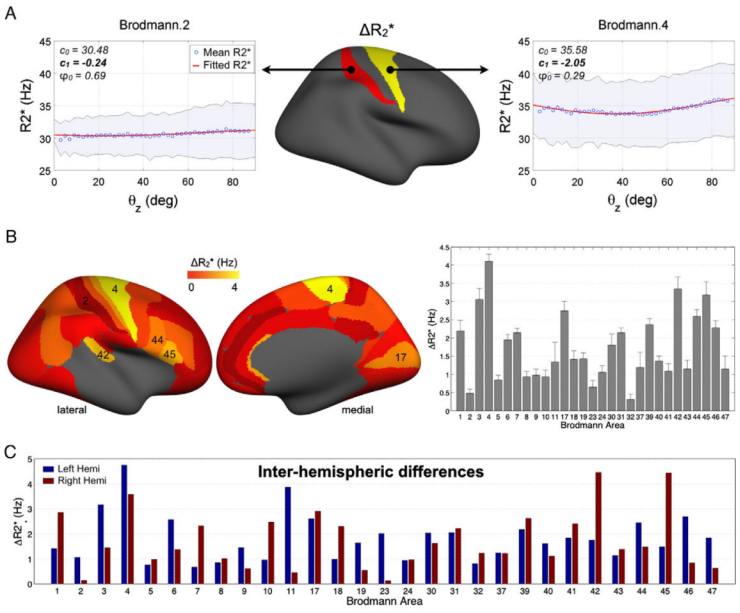

Fig. 5.

A. R_2* versus θ_z in two regions of the cortex defined by the Brodmann atlas (BA2 and BA4). For visualization, R_2* values were averaged by bins of 2 θ_z across all subjects (hence 45 bins in total). Standard deviation is displayed as light blue. Fitting curve is overlaid in red and fitting parameters are indicated at the top left of each figure. B. Dependence towards B_0 across Brodmann areas. $R_2^*(\theta_z)$ was fitted for every vertices within each Brodmann area, and the resulting ΔR_2* is displayed for each area. The maximum B_0 dependence occurred in the primary motor cortex, with ΔR_2*=4.10 Hz. The bar graph shows quantitative values of ΔR_2*, with error bars corresponding to the 95% confidence bounds. C. Comparison of ΔR_2* estimates across hemispheres.

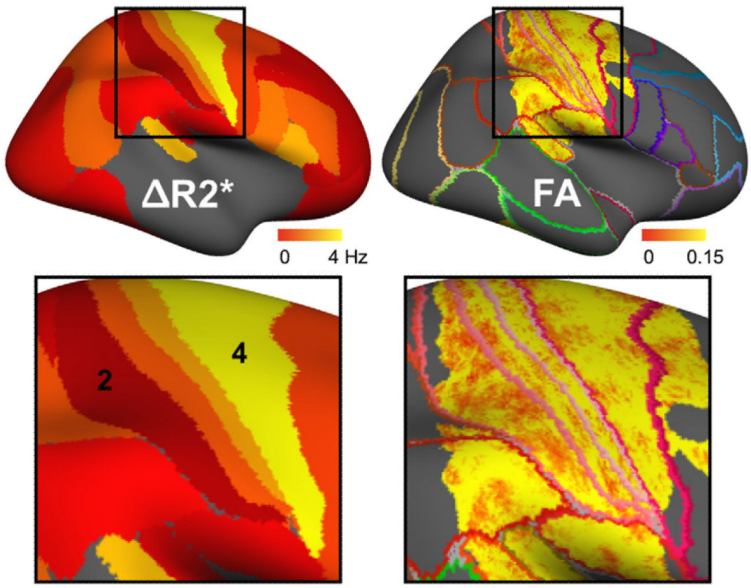

Fig. 6.

Map of B_0 orientation dependence (ΔR_2^*) and fractional anisotropy (FA) map estimated from DTI data, normalized to the same fsaverage template and averaged across subjects (N=6). Higher ΔR_2^* is associated with higher FA in BA4 (motor cortex), and lower ΔR_2^* is associated with lower FA in BA2 (sensory cortex), suggesting higher coherence of myelinated fibers in the motor cortex. Note that the field of view was reduced in the DTI acquisition, due to acquisition time constraints, precluding the study of the whole cortex.